Non-Prismatic Sub-Stiffening for Stiffened Panel Plates — Stability Behaviour and Performance Gains

Quinn, D., Murphy, A., McEwan, W., & Lemaitre, F. (2010). Non-Prismatic Sub-Stiffening for Stiffened Panel Plates — Stability Behaviour and Performance Gains. Thin-Walled Structures, 48(6), 401-413. DOI: 10.1016/j.tws.2010.01.010

Published in:
Thin-Walled Structures

Document Version:
Peer reviewed version

Non-Prismatic Sub-Stiffening for Stiffened Panel Plates – Stability Behaviour and Performance Gains

D. Quinn[a], A. Murphy[a,*], W. McEwan[a] and F. Lemaitre[b]

[a] *School of Mechanical and Aerospace Engineering, Queen's University Belfast, Ashby Building, Belfast. N. Ireland, U.K. BT9 5AH*

[b] *Unité Aéronautique et Laminés Technique, Centre de Recherche de Voreppe Centr'Alp, BP 27, 38341 Voreppe Cedex France*

Abstract (limit 100)

Previous work has demonstrated the potential to introduce plate element sub-stiffening to increase the local stability and thus static strength performance of integrally machined aluminium alloy stiffened panels. The introduction of plate element prismatic sub-stiffening modifies local plate buckling behaviour and within realistic design constraints, may produce sizable performance gains with equivalent mass designs. This article examines through experimental and computational analysis the potential of non-prismatic sub-stiffening for tailoring local plate stability performance. Using non-prismatic sub-stiffening, the experimental work demonstrates potential initial buckling performance gains with equivalent mass designs (+185%), and computationally, potential mass savings with equivalent static strength performance designs (–9.4%).

Keywords: Panel buckling, Sub-stiffening, Machined panels, Panel testing.

*** Corresponding author:** Tel.: +4428 9097 4095; fax: +4428 9066 1729. E-mail address: a.murphy@qub.ac.uk (Adrian Murphy).

1. Introduction

1.1 Background

The structural configuration of transport vehicles typically includes the use of stiffened panels given their design potential for combined lightweight with high strength and stiffness. Stiffened panel structures generally comprise an external plate, divided and supported longitudinally and laterally by internal stiffeners. Additional weight-savings are possible if the sub-divided plate elements are allowed, and design to locally buckle at load levels below the ultimate required capacity of the structure. This characteristic is due to the stable post-buckling response of stiffened panels to compression and shear loading. The longitudinal and lateral stiffeners then carry additional loading to reach the ultimate capacity of the structure. Stiffened panel structures are therefore frequently designed with elastic plate buckling at load levels expected in-service or with plastic plate buckling at the maximum in-service loads and for ultimate collapse at factored load levels, which consider in-service loading plus an appropriate safety factor.

Recent advances in the strength and damage tolerance characteristics of available materials offer opportunities for increased stiffened panel working and limit stresses, for example with next generation Aluminium-Lithium alloys [1]. To design to these higher working stresses it is on occasion desirable to increase the local panel plate element stability without increasing the volume of material at the cost of increased manufacturing complexity. Such improvement in local plate buckling performance is plausible by introducing plate element sub-stiffening [2]. The concept of plate sub-stiffening relies on the introduction of local plate element structural features which transform the plate into a panel and which if design correctly will result in increased stability.

By selective local plate sub-stiffening, static and life performance may be effectively tailored allowing the potential for greater panel working stresses, corresponds with recent advances in available materials. What is more, Bushnell and Rankin [3] demonstrated that including small sub-stiffeners between the conventional primary stiffeners 'can not only lead to an increased buckling resistance, but more importantly to a much more robust optimum in terms of stiffener pitch'. Additionally, the damage tolerance characteristics of stiffener panel structures may be improved by the addition of plate element features designed to retard fatigue crack growth [4–7]. Considering panel post-buckling, improved plate stability should translate into improved collapse performance. Higher initial plate buckling stresses alone will result in improved load carrying ability of the plate bays within the post-buckled domain. In addition, higher initial buckling stresses could result in larger effective plate zones working with the longitudinal stiffener within the post-buckling domain and therefore higher critical ultimate stresses and panel loads.

1.2 Previous work – Prismatic sub-stiffening

The concept of stiffened panel sub-stiffening has previously been experimentally demonstrated for 'thin', moderately loaded, post-buckling aerospace applications [8]. The experimental work focused on specimens with three longitudinal stiffeners and examined prismatic sub-stiffening concepts under uniform compression. To this end, two aluminium alloy specimens were designed, manufactured and tested with the same primary stiffener configuration and primary stiffener cross-section designs, as well as the same global length, width and masses (within 0.027 Kg, 1.35%). The sub-stiffener designs were constrained with manufacturing and damage tolerance minimum thickness and maximum height constraints. The experimental work demonstrates the potential to improve plate element stability. For the particular geometry and material tested a initial plate buckling performance gain of +87.2% and resultant panel post-buckling collapse gain of +17.7% were found. Further numerical

studies aimed to evaluate if equivalent behaviour and performance gains were achievable when applied to larger structures consisting of recurring panels (unconstrained by experimental boundary conditions). Expansion of original specimen designs to larger panel structures suggest marginally lower performance gains (65.9% and 6.8% for initial buckling and collapse performance respectively) due to the change in plate element boundary conditions from clamped to simply supported. Finite Element simulations of sub-stiffened versus conventional designs also demonstrated potential mass savings of 15.6% for equivalent static strength performance.

1.3 Design and analysis tools

Given the practice of allowing the plate elements between stiffeners to buckle at a percentage of the ultimate load, the ability to accurately predict the local buckling, post-buckling and failure behaviour of stiffened panel designs is essential. The general theory of buckling and post-buckling behaviour is well established [9, 10]. The conventional analysis methodologies apply combinations of empirical and semi-empirical plate and column design formulae [11-13]. The formulas are extended to cover stiffened panels by applying simplifying assumptions, which allow the division of the structure into plate and column sub-components. These currently used empirical and semi-empirical plate and column design formulae are not necessarily validated or appropriate for stiffened panels with plate sub-stiffening. Therefore, not only is the understanding of the behaviour of sub-stiffened post-buckling panels required but validated buckling performance prediction methods are also needed for individual sub-stiffening configurations.

1.4 Research objectives

The concept of plate element sub-stiffening for static strength performance gains relies on the introduction of structural features, which modify the initial plate buckling behaviour of

stiffened panels. For focused aircraft applications, this concept has been validated experimentally and computationally for prismatic sub-stiffening concepts under uniform compression. The aim of the work documented within this article is to expand this knowledge and demonstrate static strength performance gains attained with non-prismatic sub-stiffening on representative aircraft panels. The experimental work focuses at the sub-component level, examining multi stiffener panels between transverse stiffeners. Additional Finite Element simulation studies focus on evaluating potential performance gains when applied within larger panel structures. The present study focuses on integral metallic specimens, manufactured by standard subtractive machining methods. The work presented herein is part of a larger research program that is investigating potential sub-stiffening concepts, manufacturing methods and developing design and analysis tools.

2. Specimen design and manufacture

2.1 Background

As noted in the introduction, previous research work focused on the static strength performance of stiffened panels under uniform compression loading with simple prismatic sub-stiffening concepts. Under pure compression loading, introducing features that longitudinally stiffen potentially offers the greatest overall benefit. Longitudinal prismatic sub-stiffening was shown to modify local plate buckling behaviour and this behaviour could, within realistic design constraints, result in sizable performance gains with equivalent mass designs. However, aircraft stiffened panels typically have to cope with a variety of loading conditions, normally including combinations of destabilising compression, both laterally and longitudinally, shear and normal loading. Hence, the introduction of off-axis sub-stiffeners is of great interest for tailoring to the particular loading environment.

Gurdal et al [14 - 17] introduced curvilinear fibres within a laminate, allowing in-plane and bending stiffness to be locally tailored. They proposed that the tailoring of load paths could produce more favourable stress distributions and lead to improved structural performance. Studies on simply supported square plates under axial compression [14] demonstrated that the optimum orientation depends on the particular structural application – for a plate under compression the axial stiffness is maximised when the fibres at the centre of the plate are orientated at 0° to the loading axis. In contrast, for optimal buckling performance the fibres at the centre of the plate should be orientated at ±45° to the loading axis. Clearly a trade-off between axial stiffness and off-axis stiffness is required for an optimal design for a given loading combination and critical failure behaviour [17].

Considering metallic structures, off-axis stiffeners have existed in the form of isogrid or grid stiffened configurations for decades [18]. The isogrid panel design is essentially aimed at providing base isotropic skin stiffness that is strengthened locally by stiffener elements aligned for specific loading configurations. Collier [19] and Baker [20] have recently studied the application of grid stiffened structures for space shuttle and helicopter applications respectively. The grid stiffened structures are utilised to deal with particularly complex load configurations, where loading in various directions are of equivalent magnitude. The outcome is typically a rigid design with high out-of-plane bending stiffness. With regards to plate buckling, the plate bays between the grid stiffened structures are typically smaller than those found within conventional stiffened panels, moreover the high levels of rotational restraint offered by the rigid framework can contribute to higher local plate buckling performance. Assuming the use of a single stiffener design within the panel, for any post-buckling performance, the stiffener planform must be designed with sufficient stiffness to act as skin buckling pivot lines.

Research by York [21] highlights the key relationship between the stiffened planform and the associated stiffener mass. By analysis, York observed that hexagonal stiffened arrays provide a lighter alternative while offering improved buckling performance over a "square" planform. York also highlights the importance of the planform orientation with respect to the loading axis. For pure axial compression the studies indicate buckling performance gains of up to 20% are possible when square grid stiffened planforms are orientated at 45° to the loading axis.

Kapania [22] examined the influence of orientated stiffeners on the buckling performance of a simply supported flat plate. The study involved size optimisation of a number of arbitrary design configurations to evaluate potential mass savings with regards to stiffener spacing, orientation and curvature. While the study was limited to pure shear loading a number of interesting observations were made; the distribution of higher flexural bending stiffness across the plate is more beneficial than concentrating it at a particular location, localised areas of high bending stiffness, should be located near to the point where maximum out-of-plane displacement is anticipated to occur. The plate designs within the study have little or no post-buckling strength on their own, however if considered as a sub-stiffened plate within a traditional stiffened panel, the potential for post initial buckling behaviour is possible.

Murphy et al. [23] and Özakça et al. [24] briefly report on a parametric analysis undertaken on a metallic stiffened panel with curvilinear sub-stiffeners. Predicted buckling performance gains of up to 450% were numerically demonstrated with optimal curvilinear stiffeners aligned at 0° to the compression loading axis at the loading edges, and intersecting at 30° to 45° to the loading axis at the plate bay centres. Finally, it is worth noting Young's [25] and Klinzmann's [26] investigations, which highlight a number of design issues associated with orientated stiffeners. Studies on a single orientated stiffener on a flat plate indicated

significant levels of transverse loading on the plate, which had a detrimental impact on structural performance.

In summary, locally tailoring the directional stiffness of a plate can potentially yield high initial buckling performance. Either the improved performance can arise because of a grid stiffened planform design remaining in-plane, forcing initial buckling to occur between the grid stiffeners, or alternatively, the grid stiffened planform can increase the plate bending stiffness, increasing the plate's overall resistance to buckling. The influence of plate bay variable stiffness and resulting panel post-buckling performance is largely undocumented. The literature has however highlighted the trade-off between loss in axial stiffness and the potential increase in initial buckling performance for off-axis stiffening.

To assess the potential benefits and issues surrounding the use of off-axis stiffeners as plate element sub-stiffening, a series of aluminium alloy specimens are designed, manufactured and tested. One specimen with conventional uniform thickness plate elements, Specimen A, and one with off-axis plate element sub-stiffening, Specimen E. Both specimens have the same primary stiffener configuration and primary stiffener cross-section designs, as well as the same global length, width and mass (within 0.029 Kg, 1.4%).

2.2 Specimen A

The conventional specimen design represents a typical prismatic aircraft panel in operation, against which the relative performance of the sub-stiffened specimen may be referenced. The specimen was designed to represent typical fuselage stiffened panel geometry, with multiple plate bays over a single lateral stiffener (frame) pitch. Additional design recommendations were imposed to allow the results to be compared with previous tests. The specimen design requirements included target stiffening ratios and the inclusion of pad-ups under primary stiffeners to facilitate future potential manufacturing processes such as laser beam welding as

well as available material stock size and basic damage tolerance constraints. As the primary focus of the analysis is plate stability behaviour, complex stiffeners were avoided by designing the specimen to include blade stiffeners only. The design process considered three potential configurations with various test set-ups. Using conventional analysis procedures [11–13] the proposed test setups are evaluated and the most appropriate configuration selected and the design fine tuned to meet all design requirements. The selected configuration resulted in two central skin bays and two edge bays separated by the stiffeners, Fig.1. The edge plate bay geometry was sized such that initial edge bay plate buckling would occur at a marginally higher stress than that of the central bays. Experimentally this arrangement is aimed at preventing premature failure of the specimen edge stiffeners.

2.3 Specimen E

Initially a number of individual sub-stiffener profiles were investigated and a simple blade sub-stiffening profile selected for its manufacturing simplicity, its potential for non-complex sub-stiffening intersections, and its compatibility with previous prismatic sub-stiffening work [8]. A number of non-prismatic sub-stiffening planforms were then considered, inspired by the curvilinear patterns previously developed for metallic panels [24] and tow-steered composite panels [17]. However, preliminary manufacturing simulations indicated significant additional machining time due to the high number of acute angles sub-stiffener intersections, or additional panel mass with the introduction of larger than structurally required intersection rads. Thus considering manufacturability for this demonstration, a number of simplified sub-stiffening configurations were developed based on the curving crossing pattern concept. Considering a series of manufacturing minimum thicknesses and maximum height constraints for the sub-stiffeners, along with target total machining time (based on the predicted baseline specimen total machining time) a single configuration was selected and fine-tuned, Fig. 1.

As with the conventional specimen (Specimen A) the design consists of three primary stiffeners, identical in profile and pitch to Specimen A, with each plate bay stiffened by a combination of ±45° and 0° angle sub-stiffeners. The 0° sub-stiffeners are not equally spaced but positioned such that they run directly into the 45° sub-stiffener planform located within the central zone of the bay. To allow the introduction of the sub-stiffeners with no additional mass the selected design resulted in a reduction of plate thickness (when compared to the conventional specimen, Specimen A). Specimen E's detailed sub-stiffening topology was defined such that the critical buckling stress of the plate 'sub-bays' was greater than the critical buckling stress of the conventional specimen plate bay. Given the applied machining and damage tolerance constraints it was not possible to have identical specimen masses and meet all other design constraints. Hence Specimen E's design is marginally lighter (0.015 Kg, 0.76%) than Specimen A's, Table 1.

2.4 Specimen manufacture

The specimens were machined from 50 mm thick 2024-T351 aluminium alloy plate. Each specimen, once machined, was accurately measured to assess machining precision. The specimen plate sections, primary and sub-stiffeners were scanned for initial geometric imperfections and each specimen was accurately weighed, Table 2. The variations in specimen mass between the designed and manufactured, and between each specimen, are associated with small in magnitude but widespread geometric inaccuracies. For example, on Specimen B the designed stiffener thickness was 2.8 mm, while the measured manufactured thickness was 2.803 mm. This example typifies the achieved machining precision, with all specimen sections marginally thicker (less that 1%) than specified within the design.

Fig. 2 presents the form of the measured geometric imperfections. Analysing the magnitude of the curvature parallel to the primary stiffeners – the maximum out-of-plane magnitude is

10.5% of the plate thickness measured from the specimen edge to the specimen centre for Specimen A and 21.1% for Specimen E (all percentages based on Specimen A's plate element thickness for consistency).

3. Experimental and computational analysis

3.1 Experimental procedure

Before testing, a 42 mm deep reinforced epoxy resin base was cast onto each specimen loading end – producing clamped boundary conditions. Once cast each specimen was strain gauged and painted in preparation for test. Gauges were located to assist in the determination of initial plate buckling and post-buckling collapse behaviour. Two calibrated displacement transducers, one either side of the specimen, were used to measure specimen end-shortening. A three-dimensional Digital Image Correlation (DIC) system was used to capture plate deformation behaviour during the tests. The specimens were tested in a 500 kN capacity hydraulic testing machine. The specimens were loaded monotonically, in displacement control, at a rate of 0.40 mm per minute until failure occurred. Load, deflection, strain data and DIC images were automatically recorded at 2-second intervals.

3.2 Finite Element simulation

Using the Finite Element method and employing non-linear material and geometric analysis procedures it is possible to predict accurately the initial buckling, post-buckling and collapse behaviour of stiffened panel [27]. The applied structural idealisation, element and mesh selection, material modelling and solution procedures are presented in detailed within the preceding paper [8]. Two sets of simulations are preformed, the first to validate the applied analysis procedures for non-prismatic sub-stiffening designs, and the second to expand the

gained experimental knowledge by modelling larger structures consisting of recurring panels not constrained by experimental boundary conditions.

3.2.1 Simulation procedure validation (Experimental models)

The first class of simulation represents the experimental test conditions with experimental specimen geometry and boundary conditions modelled. These simulations aim to validate the applied idealisation and analysis procedures. To model the effect of the support bases cast onto the specimen ends, the out-of-plane displacements of the model nodes within the cast areas are restrained. To represent experimental loading, uniform axial displacement is applied to the lower end of each model, while the displacement at the upper end is restrained in the axial direction. As in the experimental setup, the unloaded edges of the model are unrestrained.

3.2.2 Large panel sub-stiffening verification (Recurring panel models)

The second class of simulation represent equivalent panel and sub-stiffener geometry but applied to larger panel structure, unaffected or constrained by experimental boundary conditions. These simulations aim to expand the experimental knowledge by computationally examining sub-stiffening within larger recurring panel structures and thereby verify behaviour and performance levels. These simulations apply the validated idealisation and analysis procedures from the preceding analysis. Equivalent panel cross-sectional geometries are considered, however the models represent four longitudinal stiffener bays and three lateral stiffener bays. As in the previous simulations, uniform axial displacement (in the primary stiffener direction) is used to apply loading (at the lower end of the models) with equivalent axial restraint at the opposite end. A basic idealisation is used to represent the lateral stiffeners, with simple support constraints at the two lateral stiffener locations and at the upper and lower loading edges of the models. Unlike the experimental setup the models unloaded edges are constrained with periodic boundary conditions with appropriate rotational restraints.

3.2.3 Imperfection modelling

As inclusion of initial imperfections is of great importance when evaluating panel stability behaviour [27, 29-30] the out-of-plane distortions of the experimental specimens in their test conditions were accurately measured using a Co-ordinate Measuring Machine (CMM). This data allowed the representation of actual test specimen geometric imperfections within the appropriate simulations. For the simulations with no measured data (i.e. the recurring panel sub-stiffening verification models), the perfect mesh was seeded with an eigenmode, typically the first mode.

4. Results

4.1 Experimental results

Table 3 presents the experimentally measured initial plate buckling and ultimate specimen collapse loads for Specimen A and E. To determine the initial plate buckling, the parabolic strain differential method [31] was used with strain data from back-to-back gauges located at an identical location on both specimens. These were located at the centre of the left hand central plate bay, with the panel viewed from its un-stiffened side. The load versus end-shortening curves, illustrating specimen pre- and post-buckling stiffness are presented in Fig. 3 along with out-of-plane deformation data for the centre line of the right hand central plate bay (with the panel viewed from its un-stiffened side) at selected load levels. Finally, Fig. 4 presents fringe plots displaying the initial specimen buckling modes.

4.1.1 Specimen A

Specimen initial plate buckling occurred at 74.5 kN, 34% of the specimens ultimate collapse load, with the central plate bays buckling anti-symmetrically into three longitudinal half-

waves. For this specimen there was a plate post-buckling mode change at 42% of the specimens ultimate collapse load, when fourth half-waves developed, more or less simultaneously, in each of the central bays. In each plate bay, these four half-waves continued to grow in out-of-plane magnitude until the specimen collapsed. Considering specimen collapse, failure was by way of combined global stiffener flexure (stiffener-in) and local material yielding.

4.1.2 Specimen E

For this specimen the central plate bays initially buckled into ten half-waves at 213.5 kN (84% of specimen ultimate collapse load). Examination of the DIC out-of-plane deformation data indicates that the buckle half-waves correspond to local plate 'sub-bays' formed by the sub-stiffener planform, the sub-stiffeners acting as out-of-plane inflexion lines, Fig. 4. Strain gauge data from the sub-stiffeners indicates that the 45° sub-stiffeners also become unstable at the point of initial buckling. Despite becoming unstable, the sub-stiffeners continue to act as inflexion lines with each central bay holding ten buckle half-waves until failure. Specimen collapse occurred at 254.6 kN and involved global elastic stiffener flexure (stiffener-in) with localised material yielding of the plate bays. Strain measurements of up to 129% of material yield strain (0.02%) were recorded, occurring at the centre of a diamond 'sub-bay' closest to the interface of the 0° and 45° sub-stiffeners. This is in comparison to the maximum measured primary stiffener strain, which was measured on the plate directly below the central stiffener and of a magnitude of 89% of material yield strain (0.02%).

4.2 Computational results – Experimental models

The predicted load versus end-shortening curves obtained for the simulation seeded with both measured imperfections and eigen-mode imperfections (Fig. 2), and for both specimens are presented in Fig. 5. Table 4 presents the computationally predicted initial plate buckling and ultimate panel collapse loads. As with the experimental analysis, initial plate buckling was determined applying the parabolic strain differential method with strain data from back-to-back virtual gauges located at the same point on all specimens and models (the centre of the left hand central plate bay, with the panel viewed from its un-stiffened side). Fig. 4 presents a fringe plot of the predicted out-of-plane plate behaviour for both specimen models seeded with measured imperfections.

4.2.1 Specimen A

Both simulations accurately predict the number of initial buckle half waves. The simulation seeded with the eigen-mode imperfection predicted an overly conservative buckling load (–29%), whereas the simulation seeded with the measured imperfection marginally over predicted the initial buckling performance (+5%). Considering post-buckling behaviour, the use of the measured imperfections allows accurate prediction of mode changes observed experimentally. With the simulation predicting an increase in the number of half waves from three to four at 85.5kN (40% collapse load). In the case of the eigen-mode seeded simulation, a mode change from three to four half waves is predicted but not until 165 kN (78% collapse load).

Considering specimen collapse, both simulations produce conservative predictions within 2.3% of those experimentally measured. The predicted failure mode of both the eigen-mode and measured imperfection analysis are consistent, displaying global stiffener flexure (stiffener-in) with local material yielding, Fig. 6.

4.2.2 Specimen E

Both simulations accurately predict the number and form of initial buckle half waves (ten half-waves between the skin bay central ±45° sub-stiffeners, Fig. 4). However, both simulations under-predict the initial buckling performance – the simulation representing the measured imperfection under-predicts by –19.1 % and the simulation representing the eigenvalue imperfection under-predicting by –22.6 %.

Considering specimen collapse, both simulations produce conservative predictions, with the measured imperfection simulation under predicting by –6.2 %, and the eigen-mode imperfection simulation under predicting by –9.9 %. Both the measured imperfection simulation and eigen-mode imperfection simulation shows good agreement with the experiment final end-shortening at collapse, +1.7 % for the measured imperfection and -6.36 % for the eigen-mode imperfection. The prediction of Specimen E's failure mechanism is consistent for both seeded initial imperfection simulations, and is in agreement with experimental data, i.e. global elastic stiffener flexure (stiffener-in) with localised material yielding of the plate bays (Fig. 6). The maximum observed strain for both simulations occurs in the central 'sub-bays'. This is in contradiction to the experimental case where maximum strain occurred in the lower "sub-bays" at the interface of 45° and longitudinal sub-stiffeners. The level of maximum strain recorded in the plate bays is under-predicted for both simulations, –16.2 % for the measured imperfection simulation and –6.3 % for the eigen-mode imperfection.

4.3 Computational results – Recurring panel models

The predicted load versus end-shortening curves obtained for the recurring panel simulations are represented in Fig. 7. Design A represents the constant plate thickness cross-sectional geometry of Specimen A and Design E represents the non-prismatic sub-stiffened plate cross-sectional geometry of Specimen E. Table 5 presents the computationally predicted initial plate

buckling and ultimate panel collapse loads. Again, the determination of initial plate buckling employs the parabolic strain differential method. Fig. 8 presents the predicted initial plate buckling out-of-plane fringe plots, and Fig. 9 presents the simulation predicted collapse modes.

4.3.1 Design A

The simulation seeded with the eigen-mode imperfection predicts initial plate bay buckling with four plate half waves at 61.5 kN (36% of the ultimate collapse load) (Fig. 8) and predicts that this plate buckle waveform is maintained until collapse. Considering collapse, the simulation predicts ultimate failure as global stiffener flexure (stiffener-in) with local yielding (Fig. 9), with this occurring at 171.3 kN.

4.3.2 Design E

Considering panel buckling, the simulation seeded with the eigen-mode imperfection predicts initial buckling to occur at 143.9 kN (79% of ultimate collapse load). The initial buckling mode is in the form of asymmetric half-waves either side of the lateral supports, Fig. 8. The out-of-plane displacement is confined to the sections of the plate bays supported by the longitudinal sub-stiffeners, with the sections of the skin bays supported by the 45° sub-stiffeners remaining in-plane. Considering collapse, the simulation predicts ultimate failure at 181.8 kN in the form of global stiffener flexure (stiffener-in) with local yielding (Fig. 9).

Considering the high post-buckling ratios observed within the sub-stiffened experimental tests there is the potential for sub-stiffened panel ultimate performance to be sensitive to initial plate bay buckling behaviour. Additional simulations were therefore undertaken with global imperfections and combined local plate eigen-mode and global imperfections. These analyses confirmed that the ultimate collapse performance of the non-prismatic sub-stiffened design

was no more sensitive to global and combined local and global imperfections than the conventional panel design, Table 6.

Table 7 summarises the key measured and predicted, design and specimen loads and modes which will be discussed within the following section.

5. Discussion

5.1 Initial plate buckling behaviour

Examining the experimental results, it can be seen that the initial buckling form of a panel plate bay may be modified with the addition of sub-stiffeners. For Specimen E's design the sub-stiffening features have sufficient stiffness to enforce initial buckling to occur between the plate sub-stiffening planform. The experiments have demonstrated that the introduction of non-prismatic plate sub-stiffeners can, without adding mass to the panel structure, improve initial plate buckling performance (+186.6% for Specimen E) and therefore positively influence overall post-buckling collapse strength (+17.5% for Specimen E). It is also worth noting the reduced out-of-plane displacement approaching ultimate collapse, with a maximum displacement of 5.95 mm measured for Specimen A compared to 1.82 mm for Specimen E (at approximately 95% of specimen ultimate collapse load).

Examining the Finite Element predictions, there is excellent agreement with the experimental behaviour, with skin bay buckling forms predicted accurately. However, predicted loads with simulations seeded with measured imperfections do vary significantly from measured experimental performance. Focusing on the results from simulations seeded with eigen-mode

imperfections, initial buckling mode predictions closely mirror the experimental behaviour and appear consistently conservative.

Expansion of the analysis to larger structures consisting of recurring panels, the results confirm the potential buckling performance gains associated with plate bay sub-stiffening. However, the transition from clamped experimental edge conditions to simple support conditions at the lateral supports may also have altered the buckling form of Design E. The reduction of rotational restraint appears to have induced instability of the skin sections supported by the longitudinal sub-stiffeners adjacent to the lateral supports. Under test conditions, the skin area supported by the longitudinal sub-stiffeners was stabilised by the cast end supports, however, within the recurring panel this area becomes the critical area for initial buckling. This suggests that the transition from ±45° sub-stiffeners to 0° sub-stiffeners is a design variable which should be determined to prevent premature instability of areas adjacent to lateral supports.

5.2 Collapse behaviour

The post-buckling and collapse behaviour of the experimental specimens was predicted closely when simulations represented the specimen measured imperfections. In these cases plate buckle mode changes (Specimen A) and collapse loads were predicted within 6.25% of those experimentally measured. Predictions of Specimen A are marginally closer to experimental data than Specimen E. The simplified idealisation of complex radii at sub-stiffener interfaces resulted in Specimen E having a marginally lower volume than its experimental counterpart (-1.27%). For the simulations with eigen-mode imperfections, the experimental post-buckling behaviour was less accurately predicted for Specimen A. Specimen A mode changes, while predicted, were different in form and tended to be predicted at higher loads than were measured experimentally. Sub-stiffened specimen post-buckling and

collapse behaviour was predicted closely with the eigen-value imperfection, with the associated collapse load marginally lower than that predicted using the measured imperfection.

The expansion of the numerical analysis to larger recurring panel structures also demonstrates performance gains for the sub-stiffened designs. However, the premature buckling of the skin bays adjacent to the lateral supports on Design E may have inhibited the collapse performance.

5.3 Mass optimised design

Considering the potential performance gains achieved for the mass equivalent specimens, the validated Finite Element methods were utilised to convert performance gains into potential mass savings. A specimen redesign was undertaken, focused on modifying the skin bay geometry whilst holding the global panel dimensions and primary stiffener geometry constant. The resulting design, matched the collapse performance, while exceeding the initial buckling performance of the baseline design (Specimen A), but with a significantly reduced mass (–9.42%). Examining the variation between the "mass optimised" and mass equivalent (Specimen E) design, the mass optimised design exhibits a 13.3% reduction in the skin thickness and a 26.7% reduction in the thickness of the sub-stiffeners. The sub-stiffening topology (the distribution of off-axis and longitudinal sub-stiffening features) is identical for both the "mass optimal" and mass equivalent designs. The "mass optimised" and mass equivalent designs exhibit the same initial plate bay buckling and ultimate collapse modes. As part of this specimen redesign, a series of simulations were undertaken to assess specimen ultimate collapse performance sensitivity to plate sub-stiffener post-buckling behaviour. The study indicated that incorrect sizing of plate sub-stiffeners would allow post-buckling mode

jumps, reducing the number of plate bay half-waves, with the plate buckling across the sub-stiffeners. This type of post-buckling mode jump reduces the ultimate collapse performance potential of the panel and should thus be avoided through appropriate sub-stiffener design.

6. Conclusions

Previous work has demonstrated the potential to introduce plate element prismatic sub-stiffening to increase the local stability and thus static strength performance of integrally machined aluminium alloy stiffened panels. The work herein demonstrates, through experimental and computational analysis, the potential of non-prismatic plate element sub-stiffening to tailor local stability performance. The experimental work focused on the sub-component level and examined non-prismatic sub-stiffening concepts under uniform compression. To this end, two aluminium alloy specimens were designed, manufactured and tested. The experimental work demonstrates the potential to improve panel stability with measured initial plate buckling performance gains of +185.1% and resultant panel post-buckling collapse gains of +17.5%. Numerical studies of these experiments with the Finite Element methods indicate that with appropriate idealisations, the behaviour of sub-stiffened panels may be predicted. Further computational analysis indicates that potential mass savings (–9.4%) with equivalent static strength performance designs are possible. Finally, expansion of the numerical studies verified equivalent behaviour and performance gains when non-prismatic plate element sub-stiffening is applied to larger structures consisting of recurring panels.

Acknowledgements

The authors gratefully acknowledge the technical and financial support of Alcan CRV, Voreppe, France.

References

[1] Ph. Lequeu, A. Danielou and F. Eberl. Latest Generation of Al-Li Plate Alloys Developed by Alcan Aerospace. The 18th Advanced Aerospace Materials & Processes Conference and Exposition (AeroMat 2007), June 2007, Baltimore, Maryland, USA.

[2] Murphy A, Quinn D, Mawhinney P, Ozakça M, and van der Veen S. Tailoring static strength performance of metallic stiffened panels by selective local sub-stiffening. 47th AIAA/ASME/ASCE/AHS/ASC Structures, Structural Dynamics, and Materials Conference, 1-4 May 2006, Newport, Rhode Island, AIAA-2006-1944.

[3] Bushnell D and Rankin C. Optimum design of stiffened panels with sub-stiffeners. 46th AIAA/ASME/ASCE/AHS/ASC Structures, Structural Dynamics & Materials Conference, 18-21 April 2005, Austin, Texas, AIAA 2005-1932.

[4] Farley GL, Newman JA and James MA. Selective Reinforcement To Improve Fracture Toughness And Fatigue Crack Growth Resistance In Metallic Structures. 45th AIAA/ASME/ASCE/AHS/ASC Structures, Structural Dynamics & Materials Conference, 19 - 22 April 2004, Palm Springs, California, AIAA 2004-1924.

[5] Ehrström, J-C, Van der Veen S, Arsène S and Muzzolini R. Improving damage tolerance of integrally machined panels. The 23rd Symposium of International Committee on Aeronautical Fatigue (ICAF 2005), 6-10 June 2005, Hamburg, Germany.

[6] Boscolo M, Allegri G and Zhang X. Design and Modeling of Selective Reinforcements for Integral Aircraft Structures. AIAA Journal, Vol. 46, No. 9, September 2008.

[7] Zhang X and Li Y. Damage Tolerance and Fail Safety of Welded Aircraft Wing Panels. AIAA JOURNAL, Vol. 43, No. 7, July 2005, pp. 1613-1623.

[8] Quinn D, Murphy A, McEwan W and Lemaitre F. Stiffened Panel Stability Behaviour and Performance Gains with Plate Prismatic Sub-Stiffening, Thin-Walled Struct 2009;47(12):1457–68.

[9] Timoshenko S.P., Gere J. M., Theory of elastic stability, 2nd edition, McGraw-Hill Book Company Inc., 1961.

[10] Bulson P.S., The stability of flat plates, 1st edition, Chatto & Windus, London, 1970.

[11] Bruhn EF. Analysis and Design of Flight Vehicle Structures. 1st Edition, Tri-State Offset Company, 1973.

[12] NASA. NASA astronautics structures manual, vol. 3. NASA, Washington, US, 1961.

[13] ESDU structures sub-series, Engineering Sciences Data Units, ESDU International Ltd.

[14] Gürdal Z and Olmedo RA. Composite Laminates with Spatially Varying Fiber Orientations: Variable Stifness Panel Concept. AIAA Journal, Vol. 31, No. 4, April 1993, pp. 601-608.

[15] Gürdal Z, Tatting BF, Wuc CK. Variable stiffness composite panels: Effects of stiffness variation on the in-plane and buckling response. Composites: Part A 39, 2008, pp. 911–922.

[16] Waldhart C., Gurdal Z., Ribbens C., Analysis of tow placed, parallel fiber, variable stiffness laminates. 37th AIAA/ASME/ASCE/AHS/ASC Structures, Structural Dynamics, and Materials Conference, 15-17 April 1996, Salt Lake City, USA, AIAA-96-1569.

[17] Tatting B.F., Gurdal Z., Design and Manufacture of Elastically Tailored Tow Placed Plates. NASA Contractor Report, August 2002, NASA/CR-2002-211919.

[18] Anonymous. Isogrid Design Handbook. NASA Contractor Report, prepared by McDonnell Douglas Astronautics Company, February 1973, NASA/CR-124075.

[19] Collier C., Yarrington P., Van West B., Composite, Grid-Stiffened Panel Design for Post Buckling Using Hypersizer. 43rd AIAA/ ASME/ASCE/AHS/ASC Structures, Structural Dynamics, and Materials Conference, 22-25 April 2002, Denver, Colorado, AIAA-2002-1222.

[20] Baker D.J., Kassapoglou C., Post buckled composite panels for helicopter fuselages: Design, analysis, fabrication and testing. Presented at the American Helicopter Society, Hampton roads chapter, structures specialists meeting, Williamsburg VA US, October 2001.

[21] York C.B., Buckling Interaction in Regular Arrays of Rigidly Supported Composite Laminated Plates with Orthogrid, Isogrid and Anisogrid Planform. Journal of the American Helicopter Society, Vol. 52(4), pp.343-359, 2007.

[22] Kapania R., Li J., Kapoor H., Optimal Design of Unitized Panels with Curvilinear Stiffeners, 5Th Aviation Technology, Integration and Operations Conference (ATIO), Arlington, Virginia, September 2005.

[23] Murphy A., Quinn D., Mawhinney P., Ozakça M., van der Veen S., Tailoring static strength performance of metallic stiffened panels by selective local sub-stiffening. 47th AIAA/ASME/ASCE/AHS/ASC Structures, Structural Dynamics, and Materials Conference, 1-4 May 2006, Newport, Rhode Island, AIAA-2006-1944

[24] Ozakca M., Murphy A., Van Der Veen S., Buckling and Post-Buckling of Sub-Stiffened or Locally Tailored Aluminium Panels. 25th International Congress of the Aeronautical Sciences, 3-8 September 2006, Hamberg, Germany.

[25] Young R., Hyer M., Starnes J., Prebuckling and Postbuckling Response of Tailored Composite Stiffened Panels with Axial-Shear Coupling, 41st AIAA Structures, Structural Dynamics, and Materials Conference, April 2000, AIAA-2000-1459.

[26] Klinzmann A., Horst P., Buckling analysis of triangularly stiffened cylindrical panels and their application to aircraft structures. 49th AIAA/ASME/ASCE/ AHS/ASC Structures, Structural Dynamics, and Materials Conference, 7-10 April 2008, Schaumburg, Illinois, AIAA-2008-2121

[27] Lynch C, Murphy A, Price M, Gibson A. The computational post-buckling analysis of fuselage stiffened panels loaded in compression. Thin-Walled Struct 2004;42(10):1445–64.

[28] Anonymous. ABAQUS-Version 6.5 user's manual, Hibbitt, Karlsson and Sorenson, Inc. 2004.

[29] Hilburger MW, Nemeth MP and Starnes JH. Shell Buckling Design Criteria Based on Manufacturing Imperfection Signatures. AIAA Journal, 44, (3), March 2006.

[30] Stroud WJ, Krishnamurthy T, Sykes NP and Elishakaff I. Effect of bow-type initial imperfection on reliability of minimum-weight stiffened structural panels. NASA-TP-3263, NASA, Washington DC, 1993.

[31] Singer J, Arbocz J and Weller T. Buckling experiments: Experimental methods in buckling of thin-walled structures, 1st edition, John Wiley & Son, 1997.

Table 1.

Specimen design masses.

	Mass (kg)	Designed mass percentage difference (%)
Specimen A	1.959	---
Specimen E	1.944	- 0.766

Table 2.

Specimen manufactured masses.

	Mass (kg)	Percentage difference from design mass (%)	Manufactured mass percentage difference (%)
Specimen A	2.008	+ 2.50	---
Specimen E	1.980	+ 1.85	- 1.39

Table 3.

Experimental initial plate buckling and ultimate panel collapse loads.

	Initial plate buckling load (kN)	Ultimate panel collapse load (kN)
Specimen A	74.9	216.6
Specimen E	213.5	254.6

Table 4.

Computationally predicted initial plate buckling and ultimate panel collapse loads for the experimental specimens.

	Specimen A		Specimen E	
	Initial plate buckling load (kN)	Ultimate panel collapse load (kN)	Initial plate buckling load (kN)	Ultimate panel collapse load (kN)
Experimental Data	74.5	216.6	213.5	254.6
Measured Imperfection	78.2	212.1	172.8	238.7
Eigen-mode Imperfection	52.8	211.7	165.4	229.3

Table 5.

Computationally predicted initial plate buckling and ultimate panel collapse loads for the recurring panel models.

	Design A		Design E	
	Initial plate buckling load (kN)	Ultimate panel collapse load (kN)	Initial plate buckling load (kN)	Ultimate panel collapse load (kN)
Eigen-mode Imperfection	61.5	171.3	143.9*	181.8

* Due to inconsistent initial buckling behaviour of Design E, buckling loads are calculated from the point of maximum out-of-plane deflection on the skin bay (as before, the parabolic strain differential method was used to determine the buckling loads).

Table 6.

Ultimate collapse performance sensitive to global and combined local and global imperfections.

	Simulation of Design A			Simulation of Design E		
Imperfection	Load (kN)	Percentage different (%)	Mode	Load (kN)	Percentage different (%)	Mode
Eigen-mode	171.3	---	Stiffener flexure plus local stiffener material yielding	181.8	---	Stiffener flexure plus local stiffener and plate bay material yielding
Global	158.7	93%	Stiffener flexure plus local stiffener material yielding	171.0	94%	Stiffener flexure plus local stiffener and plate bay material yielding
Eigen-mode plus global	158.4	93%	Stiffener flexure plus local stiffener material yielding	169.9	93%	Stiffener flexure plus local stiffener and plate bay material yielding

Table 7.

Key measured and predicted, design and specimen loads and modes.

	Initial skin bay buckling			Ultimate specimen / design collapse	
Experiment / Simulation	Load (kN)	Mode*	Location	Load (kN)	Mode
Specimen A	74.5	m = 3	Between primary stiffeners	216.6	Stiffener flexure plus local stiffener material yielding
Simulation of Specimen A (Measured Imperfection)	78.2	m = 3	Between primary stiffeners	212.1	Stiffener flexure plus local stiffener material yielding
Simulation of Specimen A (Eigen-mode Imperfection)	52.8	m = 3	Between primary stiffeners	211.7	Stiffener flexure plus local stiffener material yielding
Simulation of Design A (Eigen-mode Imperfection)	61.5	m = 4	Between primary stiffeners	171.3	Stiffener flexure plus local stiffener material yielding
Specimen E	213.5	m = 10	Between skin bay central ±45° sub-stiffeners	254.6	Stiffener flexure plus local plate bay material yielding
Simulation of Specimen E (Measured Imperfection)	172.8	m = 10	Between skin bay central ±45° sub-stiffeners	238.7	Stiffener flexure plus local plate bay material yielding

Simulation of Specimen E (Eigen-mode Imperfection)	165.4	m = 10	Between skin bay central ±45° sub-stiffeners	229.3	Stiffener flexure plus local plate bay material yielding
Simulation of Design E (Eigen-mode Imperfection)	143.9	n/a	Between skin bay upper and lower 0° sub-stiffeners	181.8	Stiffener flexure plus local stiffener and plate bay material yielding

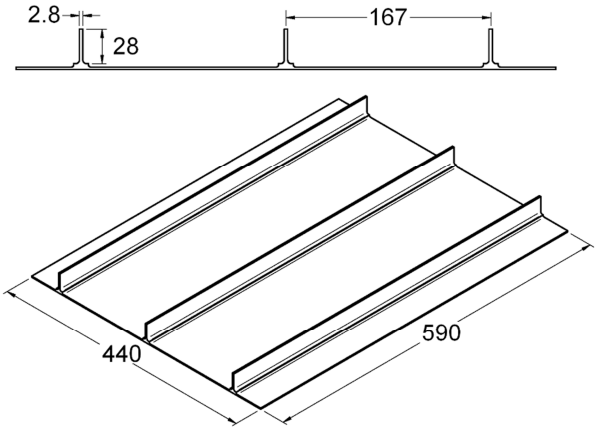

a) Specimen A

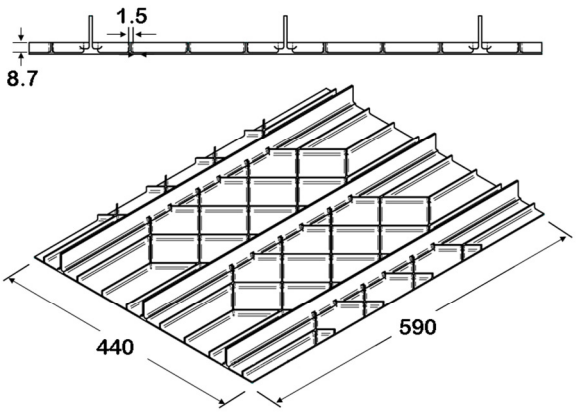

a) Specimen E

Fig. 1. Test specimen geometry.

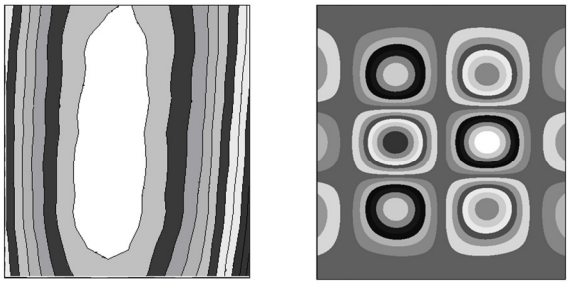

a) Specimen A

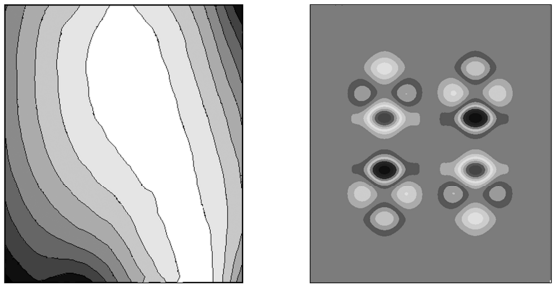

b) Specimen E

Fig. 2. Specimen imperfections.

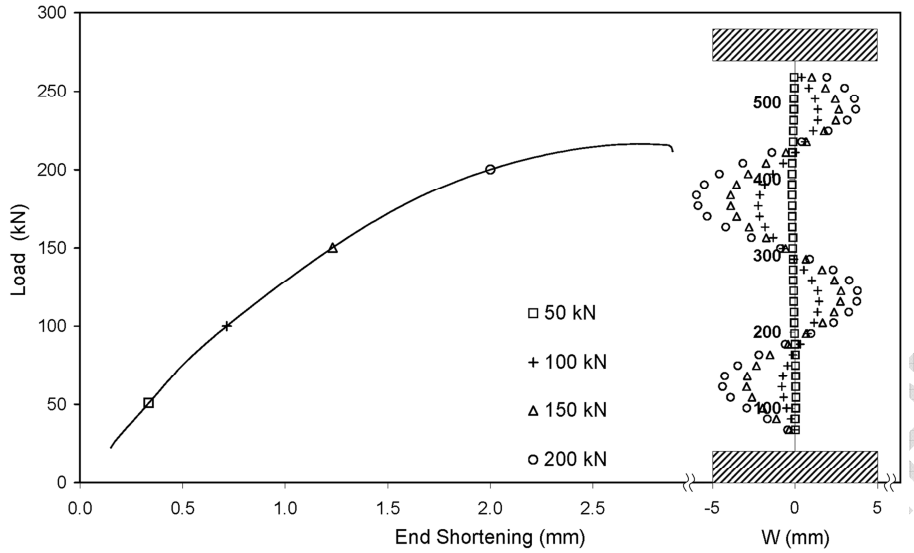

A) Specimen A

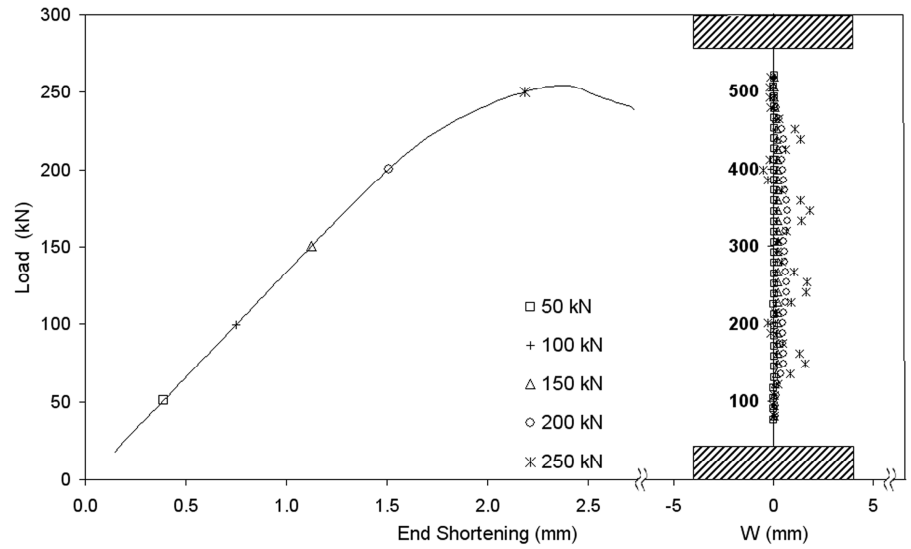

B) Specimen E

Fig. 3. Experimental load versus end-shortening curves along with out-of-plane deformation data for the centre line of the right hand central plate bay (with the panel viewed from its un-stiffened side) at selected load levels.

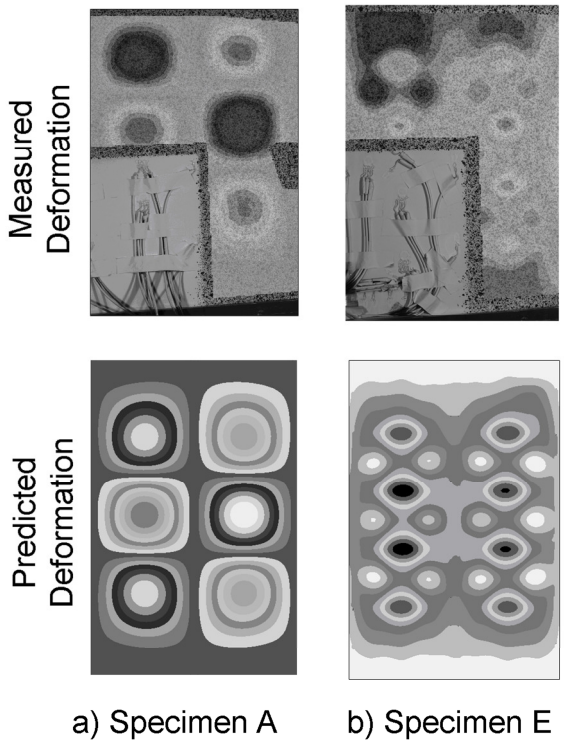

Fig. 4. Experimental and predicted out-of-plane deformations for Specimen A and Specimen E central skin bays.

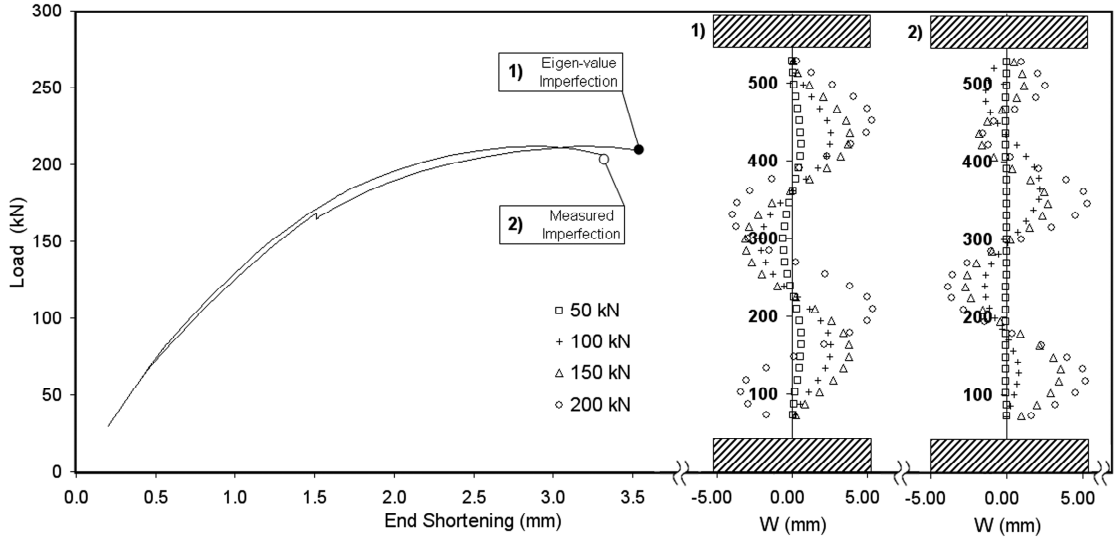

a) Specimen A

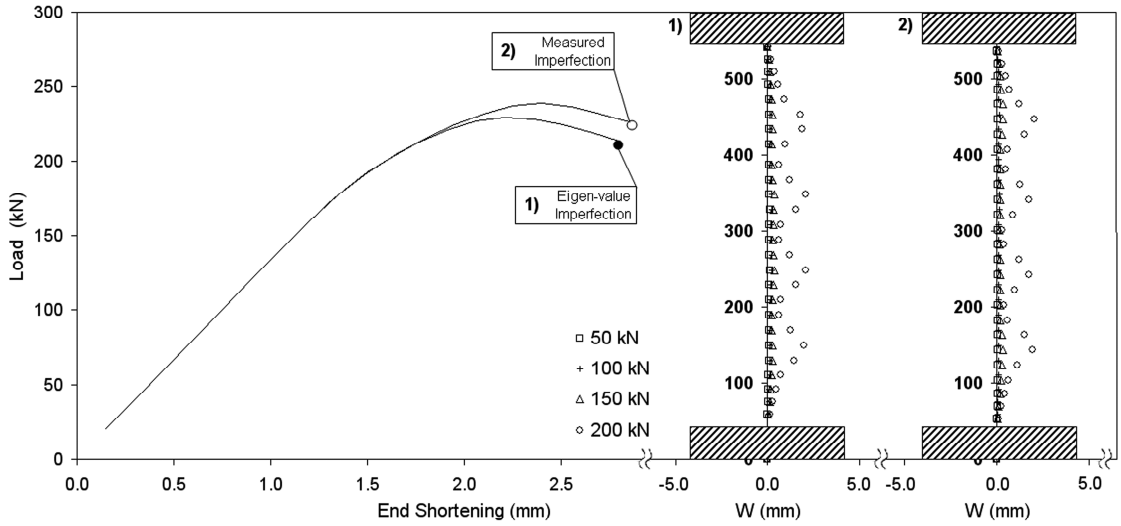

b) Specimen E

Fig. 5. Predicted Specimen load versus end-shortening curves seeded with 1) measured initial geometric imperfections and 2) fundamental eigen-mode initial geometric imperfection. Also presented is out-of-plane deformation data for the centre line of the right hand central plate bay (with the panel viewed from its un-stiffened side) at selected load levels.

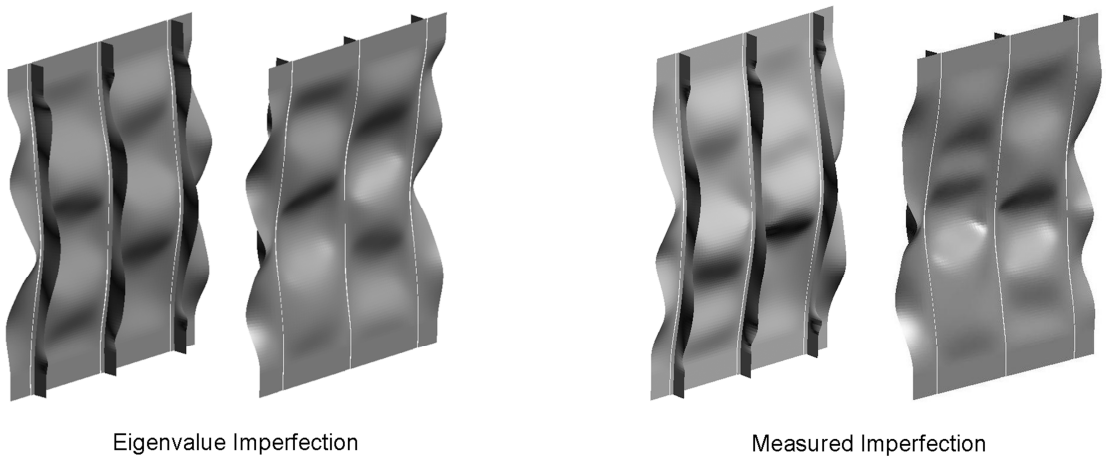

a) Specimen A

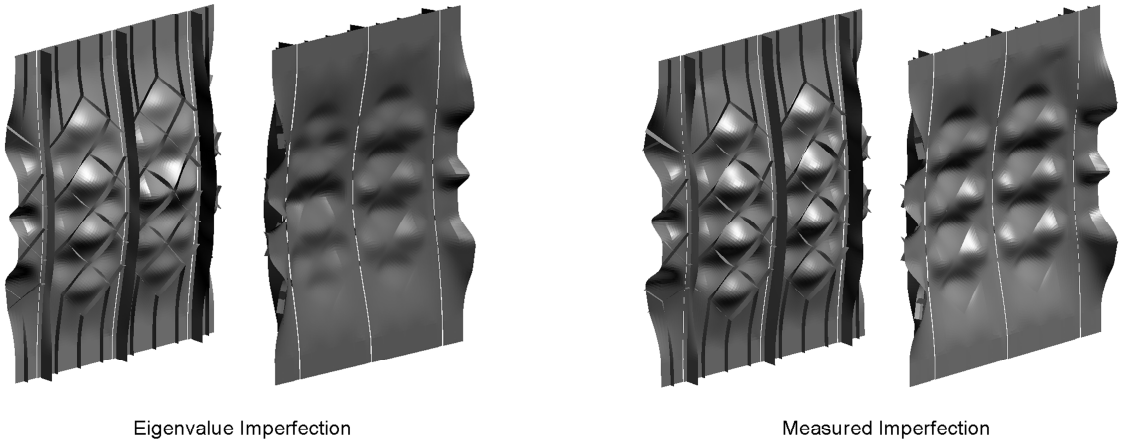

c) Specimen E

Fig. 6. Specimen simulation predicted collapse modes.

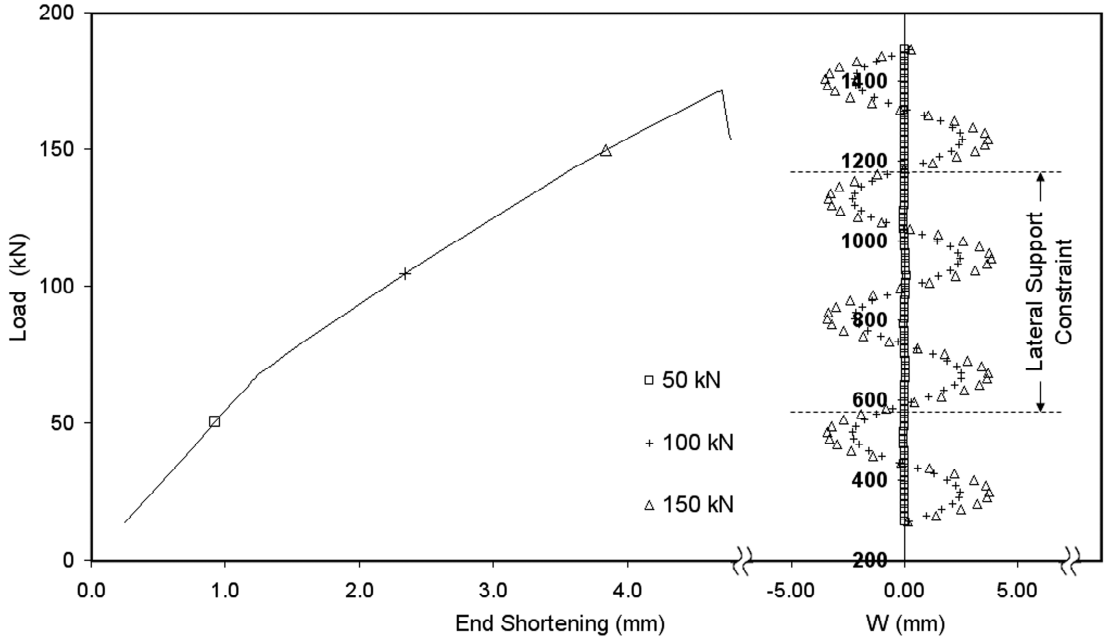

a) Design A

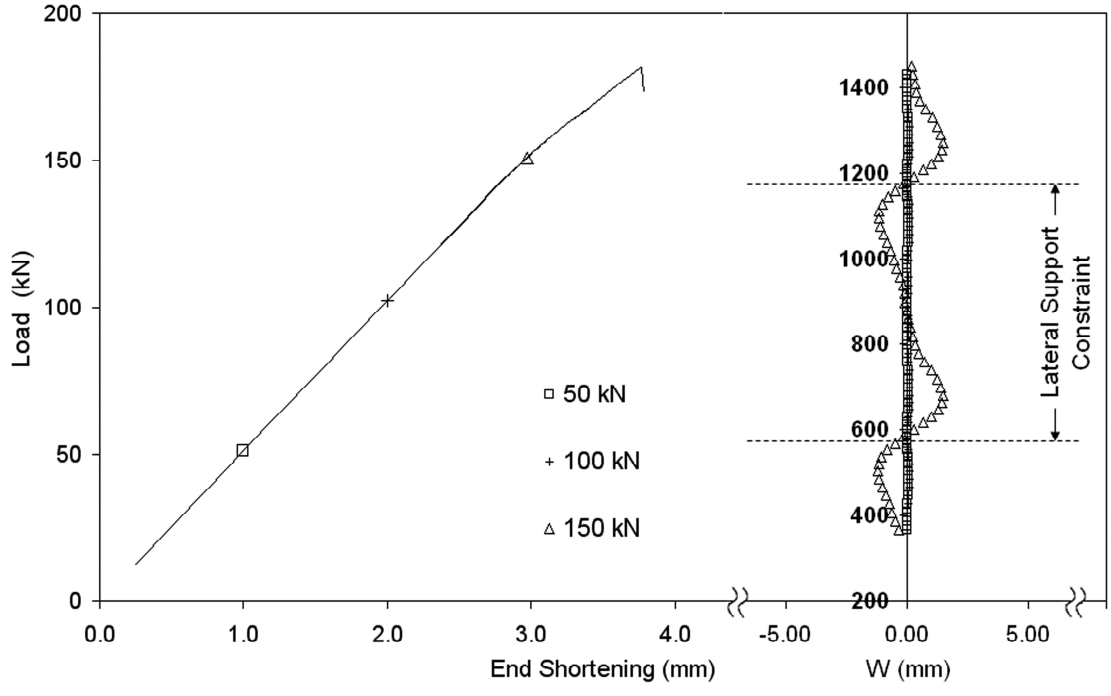

b) Design E

Fig. 7. Recurring panel models load versus end-shortening curves along with out-of-plane deformation data for the centre line of the right hand central plate bay (with the panel viewed from its un-stiffened side) at selected load levels.

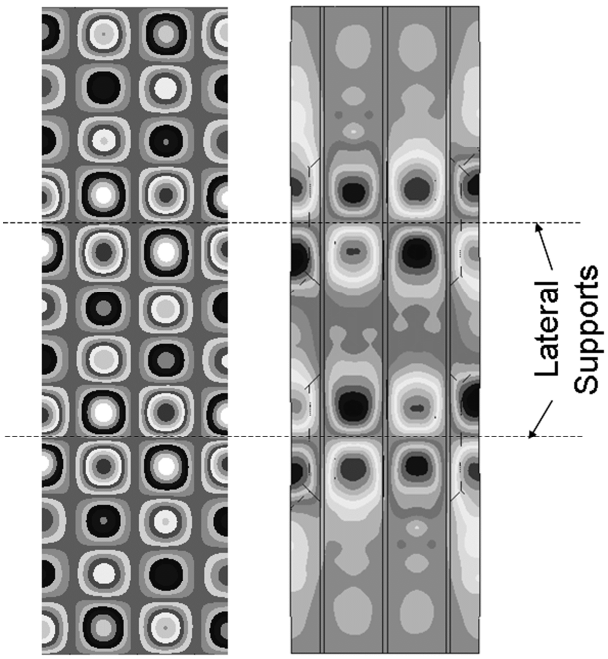

Fig. 8. Recurring panel models predicted initial buckling out-of-plane deformations.

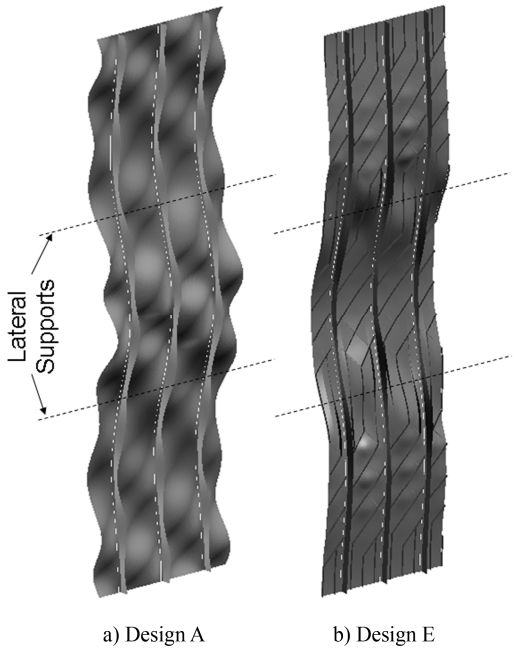

Fig 9. Recurring panel predicted collapse modes.